Research Square

Preprints are preliminary reports that have not undergone peer review.
They should not be considered conclusive, used to inform clinical practice,
or referenced by the media as validated information.

Spatial transcriptomic profiling of vascular compartments of chronic antibody-mediated rejection in kidney allografts identified compartment-specific signatures: a pilot study

Sung-Eun Choi
National Health Insurance Service Ilsan Hospital
Je-Gun Joung
CHA University
Sohyun Hwang
CHA Bundang Medical Center, CHA University School of Medicine
Tae Heon Kim
CHA Bundang Medical Center, CHA University School of Medicine
Minseob Eom
Yonsei University Wonju College of Medicine
Minsun Jung
jjunglammy@yuhs.ac

Yonsei University College of Medicine

Article

Keywords: Chronic antibody-mediated rejection, donor-specific antibody, GeoMx DSP, kidney transplantation, molecular pathology, spatial transcriptomics

Posted Date: August 18th, 2026

DOI: https://doi.org/10.21203/rs.3.rs-10222591/v1

License: This work is licensed under a Creative Commons Attribution 4.0 International License.
Read Full License

Additional Declarations: No competing interests reported.

Abstract

Despite being a major cause of kidney allograft failure, compartment-specific molecular signatures underlying chronic active antibody-mediated rejection (CAMR) remain incompletely characterized. We used GeoMx digital spatial profiling (18,677 genes) to analyze transcriptomic differences in glomeruli, peritubular capillaries, and vessels from four renal allografts with varying donor-specific antibody (DSA) and rejection statuses, and one control. Linear mixed model analysis identified differentially expressed genes enriched in antigen processing and presentation in CAMR versus non-CAMR, with major histocompatibility (MHC) class II predominating in glomeruli. Three genes (*C1QA, CTSS, IFI30*) were commonly upregulated in both compartments. Banff Human Organ Transplant pathway scores for antibody-mediated rejection were significantly elevated across all compartments in CAMR. Comparison of DSA-positive versus DSA-negative CAMR revealed enrichment of antigen processing pathways across all three compartments. Cell type deconvolution demonstrated increased macrophages in glomeruli and myeloid dendritic cells in peritubular capillaries in CAMR. Together, these findings demonstrate compartment-specific transcriptomic signatures in CAMR microvasculature and highlight mononuclear phagocytes as key drivers of antigen presentation in chronic rejection. These findings are exploratory given the limited sample size and require integration with other transcriptomic datasets.

Introduction

Chronic active antibody-mediated rejection (CAMR) is a major cause of graft loss. Moreover, due to the unresolved aspects of its pathophysiology, no established treatment exists[1]. CAMR results from chronic antibody-mediated endothelial injury leading to progressive vascular remodeling, including transplant glomerulopathy, peritubular capillary basement membrane multilayering, or arterial intimal fibrosis—ultimately resulting in graft dysfunction[2]. In cases where moderate to severe microvascular inflammation is detected, defined as either glomerulitis score (g) + peritubular capillaritis score (ptc) ≥ 2 or where C4d positivity is detected, ongoing antibody-endothelial interaction is presumed[3]. In these cases, the diagnosis is chronic “active” antibody-mediated rejection (AMR). Donor-specific antibodies (DSAs) interact with the endothelium through complement activation[4], direct endothelial signaling[5], and antibody-dependent cellular cytotoxicity[6], The third pathway has been implicated in C4d-negative AMR and has only recently attracted research attention. In pursuit of more precise diagnoses, the importance of microvascular inflammation has been clarified, and a new disease entity, C4d-negative AMR, has been identified[7], through gene transcript studies.

Concurrently, gene expression studies in patients with transplants have contributed to elucidating the pathophysiology underlying AMR. This has prompted revisions and the incorporation of molecular diagnostics in the Banff classification criteria[8]. For instance, the 2017 Banff guidelines advocated the use of gene transcript results for diagnosis and management in cases where histological, immunohistological, and serological data are equivocal[9]. Nonetheless, gene expression data are

currently inadequate to replace histological diagnosis due to challenges in validation and standardization; at present, they remain complementary.

While Nanostring nCounter enables formalin-fixed paraffin-embedded (FFPE)-based gene expression analysis correlated with Banff scores[10], it cannot resolve expression patterns at the microstructural level, which limits its ability to directly associate histological findings with transcriptomic data. Furthermore, sample pooling obscures heterogeneity among structures, thereby diminishing the apparent magnitude of differences in gene expression. In contrast, Nanostring's GeoMx digital spatial profiling (DSP) analysis enables more selective analysis of gene expression at the structural level of glomeruli or microvascular compartments. This is particularly relevant for the focal lesions of CAMR, such as transplant glomerulopathy and microvascular inflammation[11, 12].

CAMR is fundamentally a microvascular disease arising from DSA-mediated endothelial injury, resulting in tissue damage and remodeling. DSAs, as circulating antibodies, traverse the bloodstream and exert their effects on the endothelium. We aimed to investigate compartment-specific transcriptomic differences in renal allograft microvessels in CAMR and those according to DSA status. Using GeoMx DSP, we analyzed gene expression within regions of interest (ROIs) targeting specific structures, such as the glomeruli, peritubular capillaries, and arteries, to characterize CAMR at the subcompartmental level.

Materials and methods

Slide preparation

Four renal allograft biopsy specimens and one control specimen were prepared for analysis. Allografts were categorized as follows: DSA-positive CAMR, DSA-negative CAMR, DSA-positive NER, and DSA-negative NER. Histopathological diagnoses were made according to the Banff 2022 classification criteria. NER cases were further stratified by DSA status to enable comparison of molecular signatures in the presence of DSA without histologic rejection, thereby representing a state of subclinical humoral sensitization, and to serve as a DSA-matched reference for the CAMR groups. DSA testing was performed using Luminex single-antigen bead assays (One Lambda, Canoga Park, CA, USA), with DSA positivity defined as mean fluorescence intensity > 1000. C4d staining was scored according to the Banff 2019 classification (0–3). The control specimen was obtained from a non-tumor portion of a kidney from a 52-year-old male with no significant medical history who underwent a total nephrectomy for renal cell carcinoma. Clinical and pathological characteristics of each allograft sample are summarized in Table 1. The 5-μm-thin FFPE tissue sections were mounted on positively charged slides for analysis.

Table 1
Clinical and demographic characteristics of the allografts

Age/Sex	**DSA+CAMR**	**DSA-CAMR**	**DSA + NER**	**DSA-NER**
	55/M	**68/F**	**44/F**	**45/M**
Native kidney disease	Hypertensive nephrosclerosis	Hypertensive nephrosclerosis	Glomerulonephritis	Glomerulonephritis
Donor type (LD/DD)	DD	LD	LD	LD
HLA MM (A/B/DR/DQ)	(0/2/2/-)	(0/0/0/0)	(0/0/0/1)	(0/0/0/0)
1st/Re-Tx	1st	1st	1st	1st
cPRA, %	63	0	8	0
ABO-i	N	N	N	N
IS regimen	Tacrolimus, MMF, prednisolone	Tacrolimus	Tacrolimus, prednisolone	Tacrolimus
At biopsy				
Post-Tx duration, months	78	122	34	0 (6 days)
Biopsy indication	For cause	For cause	For cause	For cause
SCr, mg/dL	1.09	2.09	1.43	2.04
DSA	Positive	Negative	Positive	Negative
Type	DR53		DQ6	
MFI (max)	24,550		448*	
Banff scores				
g/ptc/cg	2/2/2	3/2/3	0/0/0	0/0/0

DSA, donor-specific antibody; CAMR, chronic active antibody-mediated rejection; NER, no evidence of rejection; LD, living donor; DD, deceased donor; HLA, human leukocyte antigen; MM, mismatch; Tx, transplantation; cPRA, calculated panel reactive antibody; ABO-i, ABO incompatibility; IS, immunosuppression; SCr, serum creatinine; MFI, mean fluorescence intensity; FU, follow-up.

* The DSA-positive NER case had an anti-HLA-DQ6 MFI of 448, below the pre-specified threshold of > 1,000. However, low-level class II DSA has been associated with increased risk of antibody-mediated rejection even at MFI < 1,000, and this case was therefore retained in the DSA-positive subgroup for the primary analysis. A sensitivity analysis reclassifying this case as DSA-negative is presented in the Supplementary Material.

c4d: † Immunohistochemistry; ‡ Immunofluorescence.

Age/Sex	DSA+CAMR	DSA-CAMR	DSA + NER	DSA-NER
	55/M	68/F	44/F	45/M
t/i/v	0/0/0	0/0/0	0/0/0	0/0/0
ci/ct/cv	0/1/0	1/1/3	1/1/0	0/0/1
c4d	3†	2‡	1†	1†
ptcml	0	0	0	0
Pathological diagnosis	CAMR (transplant glomerulopathy)	CAMR	NER	NER
Post biopsy				
Treatment	Prednisolone, plasmapheresis, rituximab	Prednisolone, plasmapheresis	-	Prednisolone
Outcome (FU, months)	Functioning (36)	Graft loss (11)	Functioning (34)	Functioning (9)

DSA, donor-specific antibody; CAMR, chronic active antibody-mediated rejection; NER, no evidence of rejection; LD, living donor; DD, deceased donor; HLA, human leukocyte antigen; MM, mismatch; Tx, transplantation; cPRA, calculated panel reactive antibody; ABO-i, ABO incompatibility; IS, immunosuppression; SCr, serum creatinine; MFI, mean fluorescence intensity; FU, follow-up.

* The DSA-positive NER case had an anti-HLA-DQ6 MFI of 448, below the pre-specified threshold of > 1,000. However, low-level class II DSA has been associated with increased risk of antibody-mediated rejection even at MFI < 1,000, and this case was therefore retained in the DSA-positive subgroup for the primary analysis. A sensitivity analysis reclassifying this case as DSA-negative is presented in the Supplementary Material.

c4d: † Immunohistochemistry; ‡ Immunofluorescence.

Digital spatial profiling

Spatial profiling and sequencing were performed according to the manufacturer's protocol (GeoMx Digital Spatial Profiler; NanoString Inc., Seattle, WA, USA). Briefly, FFPE sections were deparaffinized, subjected to antigen retrieval and proteinase K digestion, and then hybridized with probes from the GeoMx Human Whole Transcriptome Atlas (18,677 genes). All five biopsy samples were co-mounted on a single slide for simultaneous transcriptomic analysis. The number of ROIs per compartment for each case is summarized in Supplementary Table S1. Nuclear staining was performed using SYTO13 (Thermo Fisher Scientific, Waltham, MA, USA), along with fluorescence-conjugated antibodies for PanCK (NanoString, number 121300310, Cy3/568 nm), CD45 (NanoString, number 121300310, Texas Red/615 nm), and CD31 (Abcam, ab215912, Cy5/666 nm). Slides were loaded onto the GeoMx DSP, and 48 ROIs were manually selected based on morphological features identified by fluorescent markers, with a relatively even distribution across three tissue compartments: glomeruli (n = 18), peritubular capillaries

(n = 15), and vessels (n = 15) (Fig. 1). To ensure transcriptomic stability, ROIs were selected to contain a minimum of 100 nuclei as determined by SYTO13 staining. Glomeruli were identified as CD31 + structures with characteristic capillary loops containing CD45 + inflammatory cells with the highest density; the ROIs were drawn to encompass the glomerular tuft only, with Bowman's capsule included only when necessary to meet the minimum nuclei threshold. To ensure selection of glomeruli with chronic injury, glomeruli with high transplant glomerulopathy (cg) scores were first reviewed on silver-stain slides, and their corresponding locations were then confirmed on the DSP scan slides by positional matching. Peritubular capillaries were defined as CD31 + linear structures in the cortical tubulointerstitial area adjacent to glomeruli, containing CD45 + inflammatory cells, and ROIs were selected from areas with the highest CD45 + cell density. Vessels were identified as CD31 + structures with distinct luminal architecture and thicker walls comprising two or more layers of smooth muscle, restricted to cortical arterioles and arteries; the ROI encompassed the full vessel wall including the adventitia. Library preparation and sequencing were performed according to the GeoMx DSP protocol. Detailed procedures are provided in **Supplementary Methods S1**.

This study was conducted in adherence to the Declaration of Istanbul on Organ Trafficking and Transplant Tourism. All procedures performed in the current study were approved by the Institutional Review Board (IRB) of CHA Bundang Medical Center, CHA University (CHAMC IRB 2024-01-025-001, approved January 25, 2024) in accordance with the 1964 Helsinki declaration and its later amendments. The requirement for formal written informed consent was waived by the IRB.

Quality control

Raw FASTQ files were processed using the GeoMx next-generation sequencing (NGS) Pipeline (v3.1.1.6, NanoString) to generate digital count conversion files. Quality control filtering and normalization were performed using the GeoMx DSP Control Center software (v3.1.2.12, NanoString). Detailed quality control metrics and ROI images are provided in **Supplementary Methods S2** and https://doi.org/10.5281/zenodo.18933255.

Data analysis

Differential gene expression (DEG) analysis

The 48 ROIs were categorized into three tissue compartments: glomerulus (n = 18), peritubular capillary (n = 15), and vessel (n = 15). DEG analysis was performed using a linear mixed model (LMM) in the lme4 package (v1.1-37) in R (v 4.5.1). The LMM (model 1) was applied to all ROIs (n = 48), with log2-transformed normalized gene expression as the dependent variable, rejection status (CAMR vs. non-CAMR), DSA status, and transplantation status as fixed effects, and patient as a random effect. The control specimen was grouped with the non-CAMR cases. Separate LMMs were conducted for each compartment. LMM analysis (model 2) was subsequently performed on 39 ROIs from four renal allografts across three tissue compartments, with rejection status as a fixed effect and patient as a

random effect. To assess the robustness of model 1, a sensitivity analysis was performed in which the original DSA-negative NER case, obtained from a biopsy on post-transplant day 6 and therefore likely to reflect ischemia reperfusion injury, was excluded. In addition, as the DSA-positive NER case had an anti-HLA-DQ6 MFI of 448, below the pre-specified threshold of > 1,000 for DSA positivity, this case was reclassified as DSA-negative NER.

To assess within-patient ROI dependency, intraclass correlation coefficients (ICC) were calculated per compartment using a one-way random effects model, with patient as the grouping variable and individual ROIs as repeated measures across all 18,677 target genes. P-values were adjusted using the Benjamini-Hochberg procedure with a false discovery rate (FDR) threshold of 10%. DEGs were defined as genes with an absolute log2 fold change greater than 0.5 (|log2FC| > 0.5) and a false discovery rate (FDR)-adjusted p-value less than or equal to 0.1.

To evaluate the impact of DSA in CAMR, gene expression was compared between DSA-positive and DSA-negative CAMR across each ROI compartment: glomeruli (n = 4 per group), peritubular capillaries (n = 3 per group), and vessels (n = 3 per group). Given the small sample size and the absence of DEGs after FDR correction, Student's t-test was used as an exploratory, hypothesis-generating approach for the DSA-positive versus DSA-negative CAMR comparison. Statistical significance was set at $p < 0.05$. DEGs were defined as those with an absolute log2 fold change (|log2FC|) > 1 and normalized expression > 4.

Gene ontology (GO) enrichment analysis

GO analysis was conducted using clusterProfiler (v4.13.4) and org.Hs.eg.db (v3.20.0). Significantly enriched GO terms in the Biological Process (BP), Cellular Compartment (CC), and Molecular Function (MF) categories were identified using the Benjamini-Hochberg correction ($p < 0.05$, $q < 0.1$. Redundant GO terms were removed using the simplify function (similarity cutoff = 0.7) based on the Wang semantic similarity method, retaining the term with the lowest adjusted p-value within each cluster.

Single-sample gene set enrichment analysis (ssGSEA)

ssGSEA was conducted using the corto package (v1.2.4) in R (v 4.5.1) with the Banff Human Organ Transplant (B-HOT) gene panel[13]. Gene expression values were z-score normalized, and pathways with ≥ 5 genes were analyzed. Normalized enrichment scores (NES) were calculated for each sample.

Spatial cell type deconvolution

Cell type deconvolution was performed using SpatialDecon with the safeTME (Safe Tumor Microenvironment) reference profile. Detailed parameter settings are described in Supplementary Methods S3. Inflammatory cell counts and proportions were calculated for each sample and visualized as stacked bar plots. Pathway scores and cell type proportions were compared across groups using the

Kruskal–Wallis test, followed by Dunn's post hoc test for pairwise comparisons. Complete DEG, GO enrichment, and cell deconvolution results are provided in https://doi.org/10.5281/zenodo.18933255.

Results

Higher expression of antigen processing and presentation-related genes was observed in the glomerular and peritubular capillary ROIs in CAMR compared to non-CAMR

When all ROIs, including controls, were categorized into three compartments (glomerulus, peritubular capillary, and vessel) and LMM analysis was performed within each compartment (model 1), 79 DEGs (14 upregulated, 61 downregulated) in the glomerulus (Fig. 2A) and 127 DEGs (21 upregulated, 104 downregulated) in the peritubular capillary (Fig. 2B) were significantly associated with the presence of CAMR compared with non-CAMR. In the vessel compartment, only four downregulated DEGs were detected in relation to CAMR presence, with no upregulated DEGs identified (**Supplementary Figure S1**). GO analysis of the upregulated DEGs in terms of BP revealed that both glomeruli (Fig. 2C) and peritubular capillaries (Fig. 2D) were commonly enriched for antigen processing and presentation ($q < 0.15$). Notably, the glomerular enrichment was associated with MHC class II-mediated processing. Three genes (*C1QA, CTSS, and IFI30*) were significantly upregulated in both compartments in the presence of CAMR (Fig. 2E). GO-BP analysis for downregulated DEGs revealed no significant term enrichment or meaningful pathway (**Supplementary Figure S2**). In the vascular compartment of CAMR, downregulated genes included those involved in calcium-dependent signaling (*EFCAB3*), transcriptional regulation (*ZBED6CL*), metabolic signaling (*GCGR*), and developmental processes (*TBXT*); however, GO analysis showed no significant enrichment. This limited number of DEGs may reflect the histological quiescence of vascular inflammation ($v = 0$) in our cohort.

GO enrichment analysis of graft-associated downregulated DEGs revealed enrichment for terms related to glomerular filtration, nephron development, and podocyte differentiation with contributing genes including *NPHS2, AQP1, KIRREL1*, and *PTPRO* in the glomerular compartment (**Supplementary Figure S3**).In the sensitivity analysis excluding the early post-transplant NER case and reclassifying the low-MFI case as DSA-negative (**Supplementary Figure S4**), the number of FDR-significant DEGs decreased across all three compartments: glomerular (2 DEGs; 1 up, 1 down, peritubular capillary (12 DEGs; 5 up, 7 down), and vascular CAMR ROIs (7 DEGs; 1 up, 6 down). Nevertheless, key CAMR-associated genes identified in the primary analysis — including CCND1 in glomeruli and HLA-DRB1, HLA-DPA1, and PECAM1 in peritubular capillaries — remained upregulated, supporting the directional consistency of the primary findings.

Mean ICC values were 0.14, 0.12, and 0.12 for glomerular, peritubular capillary, and vascular ROIs, respectively, indicating low within-patient correlation. This pattern supports the use of patient as a random effect in the linear mixed model to account for residual clustering.

Model 2 analysis expands DEG detection and reveals vascular remodeling signatures in CAMR

LMM analysis (model 2) restricted to allograft ROIs (n = 39) identified greater numbers of DEGs – 459 DEGs (84 upregulated, 375 downregulated) in glomerular ROIs (Fig. 3A) and 791 DEGs (147 upregulated, 644 downregulated) in peritubular capillary ROIs (Fig. 3B), respectively. The upregulated DEGs (Fig. 3C**&D**) reinforced or were functionally related to the GO terms enriched in model 1, except for *IFI6*, the most strongly upregulated DEG (adj. $p = 1.4\times10^{-31}$) in the glomerular compartment. For example, in the peritubular capillary, ZEB2 (adj. $p = 3.8\times10^{-15}$) and ANXA2 (adj. $p = 5.7\times10^{-17}$) were notable for their association with the endothelial-to-mesenchymal transition (EndMT) axis. Notably, *PECAM1, VIM*, and *ANXA2* were consistently upregulated in both model 1 and model 2 analyses, providing evidence of endothelial injury and EndMT within the peritubular capillary compartment of CAMR.

In the vessel compartment, where model 1 detected only four downregulated DEGs, model 2 revealed 257 DEGs (36 upregulated, 221 downregulated) in association with CAMR (Fig. 3E**&F**). GO-CC analysis of the upregulated vessel DEGs identified enrichment for collagen-containing extracellular matrix terms. Downregulated DEGs across all three compartments showed no significant GO term enrichment with a few nonspecific terms.

DSA-positive CAMR shows multicompartment upregulation of genes related to extracellular matrix remodeling and cellular stress

To investigate the effect of DSA status within CAMR, we compared ROIs from DSA-positive and DSA-negative CAMR by compartment. Due to the limited number of ROIs, no significant DEGs were identified after FDR correction. This prompted the use of Student's t-test, which revealed 302 DEGs in glomeruli (296 up, including *COL4A1*, a basement membrane component, 6 down; Fig. 4A), 136 in peritubular capillaries (128 up, including immunoglobulin-related genes, 8 down; Fig. 4B), and 274 in vessels (269 up, 5 down, Fig. 4C). Twenty-one upregulated DEGs were shared across all three compartments (Fig. 4D) and revealed enrichment of immunoglobulin-related pathways including classical pathway complement activation and immunoglobulin receptor binding (Fig. 4E**&F**).

CAMR showed elevated AMR pathway scores across glomerular, peritubular capillary, and vascular compartments

B-HOT pathway scores were calculated for each ROI and compared across groups. The corresponding AMR pathway-associated scores, including AMR[14] (Fig. 5A) and DSA-associated tissue signatures (DSAST) scores[15] (Fig. 5B)were significantly elevated in CAMR compared with NERs and controls across all compartments: glomerulus (p = 0.0017 and 0.0032), peritubular capillaries (p = 0.0063 and

0.0062), and vessels (p = 0.046 and 0.039). Similarly, MHC class II antigen presentation[13]was significantly higher in CAMR in the glomeruli (p = 0.00099) and peritubular capillaries (p = 0.0052), with a trend toward elevation in vessels (p = 0.069) (Fig. 5C). In contrast, T cell–mediated rejection (TCMR) pathway-associated (TCMR-RATS) scores[16] did not differ significantly between CAMR, NER, and controls in any compartment (Fig. 5D). No significant differences between CAMR and NER groups based on the DSA status were observed across all the pathways (**Supplementary Figure S5**).The complete B-HOT pathway scores across all compartments are presented in **Supplementary Figure S6**.

Cell type deconvolution shows distinct immune cell enrichment across CAMR compartments compared to NER and controls

Cell type deconvolution was performed on each ROI, and immune cell proportions were compared across compartments based on their classification (Fig. 6A). Across all compartments, the proportion of monocytes, macrophages, and dendritic cells belonging to the mononuclear phagocyte system was higher in the CAMR group than in the NER and control groups. CAMR cases demonstrated an increased proportion of macrophages in glomeruli (Fig. 6B) and of myeloid dendritic cells and non-classical/intermediate monocytes in peritubular capillaries (Fig. 6C**&D**). Estimated inflammatory cell counts were higher in glomerular ROIs of DSA-negative CAMR, consistent with the more severe glomerulitis score (g = 3) (**Supplementary Figure S7-S8**).

Discussion

Among the upregulated glomerular DEGs in CAMR, interferon-γ signatures genes (*HLA-DRA, HLA-DPB1, HLA-DQA1/B1, IFI30, CXCL9*) were prominent[14]. These findings, together with cell deconvolution results, suggest that glomerular HLA class II signals in CAMR largely reflect infiltrating macrophages, with possible contributions from endothelial cells[17]. *CCND1*, a cell cycle/proliferation transcript, has also been found to be upregulated in diseased glomeruli[18]. The enrichment of MHC class II-mediated antigen presentation pathways, together with a higher proportion of macrophages, may reflect the indirect allorecognition, wherein recipient APCs present processed donor antigens on self MHC class II molecules[19]. A recent large-scale single-cell transcriptomic study identified a *CXCL10+/LILRB2 +* macrophage subset derived from recipient monocytes as a key driver of rejection-associated graft injury[20]. Our pilot study may offer a complementary perspective by spatially localizing this mononuclear phagocyte-associated signal within the renal microvascular compartments, with *CXCL9* upregulation observed predominantly in glomerular CAMR ROIs, consistent with the *CXCL9/CXCL10* proinflammatory signature described by Varin et al. Notably, *IFI6*, an interferon-α-inducible gene, was the most significantly upregulated glomerular DEG in the model 2 LMM analysis (adjusted P = $1.4X10^{-21}$), possibly indicating type 1 interferon response[21]. Its emergence may reflect the exclusion of the biologically heterogenous native control from the reference group, allowing the model 2 comparison to more specifically capture rejection-associated interferon signaling.

In peritubular capillaries of CAMR, non-classical monocyte transcripts, activated endothelial markers (*PECAM1, VIM*), and upregulation of MHC class I processing genes (*TAPBP, CTSS*)[22] was observed. Notably, *VIM, ANXA2*, and *ZEB2*, a marker of endothelial-to-mesenchymal transition (EndMT), indicates endothelial damage and activation and is associated with DSA, AMR diagnosis, and graft loss[23, 24]. GO enrichment analysis of upregulated DEGs revealed that antigen processing and presentation was the most significantly enriched biological process.

Three genes-*C1QA, CTSS, and IFI30*-were commonly upregulated in CAMR versus non-CAMR in both glomerular and peritubular capillary compartments. *C1QA/B* are complement-related macrophage markers identified in multiple single-cell and spatial transcriptomic studies, aligning with our cell deconvolution results showing increased macrophage proportions[25, 26]. *CTSS* mediates MHC class II maturation in antigen-presenting cells (APCs) and has been identified as a rejection-associated gene expression in macrophages[27]. *IFI30*, a γ-interferon-inducible gene constitutively expressed in monocytes/macrophages, mediates MHC class II-related antigen processing[14]. Collectively, these findings provide evidence for MHC class II antigen processing and presentation by monocytes/macrophages in CAMR glomeruli.

Despite known interferon-γ-induced MHC class II upregulation in renal endothelium[28], our findings suggest that HLA class II expression in CAMR is more prominent in glomeruli than in peritubular capillaries, providing a spatially resolved, compartment-specific assessment of HLA class II expression within the CAMR microvasculature. This compartmentalized pattern is supported by a single-cell ribonucleic acid (RNA)-sequencing analysis of kidney allograft rejection[29]. This spatial heterogeneity may inform targeted immunosuppressive strategies addressing primary lesion sites of rejection. In the Banff diagnostic framework, microvascular inflammation scores (g + ptc) are weighted equally in AMR assessment[30]. However, our study showed preferential upregulation of endothelial injury-associated transcripts (*VIM, PECAM1, ANXA2, and ZEB2*) in peritubular capillaries rather than glomeruli, suggesting that the peritubular capillary compartment may represent an important site of endothelial injury. This is supported by a prior transcriptomic study showing that elevated ptc scores are associated with elevated AMR-associated transcripts[10].

An important observation is the discordance between histologic Banff scores and transcriptional activation states. Although DSA-negative CAMR exhibited higher glomerulitis (g3) and transplant glomerulopathy (cg3) scores compared with DSA-positive CAMR (g2, cg2), the latter exhibited more pronounced upregulation of transcripts related to cellular stress and remodeling across glomerular and peritubular capillary compartments (Fig. 4A). Similarly, despite comparable ptc scores, DSA-positive cases demonstrated enhanced expression of antibody-related (*IGHG3, IGHG4*) and antigen presentation-associated transcripts in peritubular capillaries, underscoring that lesions with similar or even lower inflammation may exhibit heightened molecular activation depending on DSA status (Fig. 4B). Transcriptomic and histologic assessments often diverge across the spectrum of Banff lesion severity[31]. In DSA-positive glomeruli, increased *COL4A1* expression, consistent with active glomerular

basement membrane remodeling, did not correlate with cg scores. This discrepancy likely reflects the distinction between dynamic transcriptional responses indicative of ongoing injury and static histologic scores representing cumulative structural damage. Furthermore, despite histologically quiescent vessels (v = 0), vascular ROIs displayed transcriptomic differences not only between DSA-positive and DSA-negative CAMR (Fig. 4C), but also in the CAMR versus NER comparison (Fig. 3E), where upregulation of smooth muscle- and ECM-associated genes was observed, suggesting molecularly defined vasculitis undetectable by conventional histology. A small subset of upregulated DEGs shared across all compartments was enriched for classical complement activation-related pathways (Fig. 4D–F), suggesting that DSA positivity may exert a convergent immune activation pressure across distinct renal microvasculature niches. Given the exploratory nature of this analysis, these findings warrant validation in larger, independent cohorts.

Since the B-HOT gene panel was published in 2019 based on microarray study results[13], subsequent validation studies have been conducted[10]. We further investigated whether the pathway scores known to be elevated in CAMR exhibit spatial differences (Fig. 5). AMR-related pathway scores, including AMR, DSAST, and MHC class II Antigen Presentation, were higher in the CAMR group across glomerular, peritubular capillary, and vascular compartments, with statistical significance in all comparisons except for the MHC class II Antigen Presentation score in vessels. The finding that CAMR exhibits higher AMR-related pathway scores and that DSAST scores do not differ between DSA-positive and DSA-negative CAMR is consistent with previous FFPE-based[10] and microarray-based studies[32]. However, our analysis demonstrates that similar trends can be captured through spatial transcriptomic analysis of kidney microvasculature rather than bulk allograft tissue. This suggests that AMR-related pathway scores may reflect molecular phenomena occurring specifically within microvascular/vascular niches rather than representing average effects across the entire tissue, including the tubulointerstitium.

This study leverages several methodological approaches that enhance the interpretability of transcriptomic data. First, we analyzed transcriptomic information at the spatial level. Second, the use of whole-genome transcript probes facilitated the detection of genes that might otherwise be obscured due to small sample sizes. Third, LMM analysis accounting for patient-specific factors enabled identification of DEGs associated with rejection and DSA positivity. In addition, our approach of subdividing and comparing kidney cortical microvasculature provided compartment-specific insights into CAMR.

The study has some limitations. The small sample size reduced statistical power and may have obscured the true association between DEGs and CAMR or DSA status. The DSA-negative NER case exhibited low-level C4d positivity, which may reflect prior DSA exposure; this limits its interpretability as a fully negative control. Additionally, DSA testing was performed using HLA class I (A, B) and class II (DR, DQ) specificities; HLA-C and HLA-DP were not evaluated, which may have resulted in underdetection of DSA in cases classified as DSA-negative. Differences in immunosuppression regimens and time post-transplant (ranging from 6 days to 122 months) across cases represent uncontrolled variables; in particular, the early post-transplant biopsy may reflect ischemia-reperfusion injury rather than a stable rejection-free state. The t-test-based DSA comparison is exploratory and hypothesis-generating only,

given the absence of FDR-significant DEGs and the very limited ROI numbers per group. Although spatial deconvolution provided insights into important inflammatory cell populations, validation through higher-resolution techniques, such as single-cell RNA sequencing, is warranted. Future studies comparing active AMR with CAMR are needed to further elucidate the underlying pathophysiology of antibody-mediated rejection. Transcripts commonly expressed in lesions without chronic features likely reflect active AMR, while those unique to CAMR may represent transcripts associated with chronic injury.

Spatial transcriptomics revealed compartment-specific enrichment of antigen processing and presentation pathways within the CAMR microvasculature, with patterns that did not mirror the corresponding histological scores. While these findings suggest the presence of spatially distinct molecular inflammatory niches in CAMR, the limited sample size necessitates cautious interpretation, and validation in larger independent cohorts is warranted.

Abbreviations

AMR
antibody–mediated rejection
APC
antigen–presenting cell
B
HOT–Banff Human Organ Transplant
CAMR
chronic active antibody–mediated rejection
DEG
differentially expressed gene
DSP
digital spatial profiling
DSA
donor–specific antibody
DSAST
donor–specific antibody–associated tissue signatures
EndMT
endothelial–to–mesenchymal transition
FFPE
formalin–fixed paraffin–embedded
FDR
false discovery rate
GO
gene ontology
HLA
human leukocyte antigen

IRB
Institutional Review Board
LMM
linear mixed model
LOQ
limit of quantification
MHC
major histocompatibility complex
NER
no evidence of rejection
NES
normalized enrichment score
NGS
next–generation sequencing
ROI
region of interest
ssGSEA
single–sample gene set enrichment analysis
TCMR
T cell–mediated rejection
TCMR–RATS
T cell–mediated rejection–related acute tissue signatures

Declarations

Disclosure

The authors of this manuscript have no conflicts of interest to disclose.

Funding statement

This research was supported by a grant from the Research Driven Hospital R&D project, funded by CHA Bundang Medical Center (grant number: BDCHA R&D 2023-004) to Sung-Eun Choi. This work was also supported by the National Research Foundation of Korea (NRF) grant funded by the Korean government (MSIT) (RS-2024-00341570) to Minsun Jung.

Acknowledgements

I would like to express my gratitude to Jinseob Kim and his colleagues at Zarathu Co., Ltd., for their advice on data analysis and statistical processing.

Data availability

The GeoMx DSP spatial transcriptomics datasets generated and analysed during the current study are available in the Gene Expression Omnibus (GEO) repository, under accession number GSE342778 (https://www.ncbi.nlm.nih.gov/geo/query/acc.cgi?acc=GSE342778). Additional analysis results are available in Zenodo at https://doi.org/10.5281/zenodo.18933255.

Author Contributions

Conceptualization: S.Choi

Data curation: S.Choi

Formal analysis: S.Choi, J.Joung

Funding acquisition: S.Choi

Investigation: S.Choi, S.Hwang, J.Joung, M.Jung

Methodology: S.Hwang, J.Joung, M.Jung

Project administration: S.Choi, T.H.Kim

Resources: S.Choi, M.Eom, M.Jung

Software: S.Choi, J.Joung

Supervision: J.Joung, M.Jung

Validation: S.Choi, S.Hwang, J.Joung, M.Jung

Visualization: S.Choi, J.Joung, M.Jung

Writing – original draft: S.Choi

Writing – review & editing: all authors.

Approval of final manuscript: all authors

References

1. Schinstock, C. A. et al. Recommended Treatment for Antibody-mediated Rejection After Kidney Transplantation: The 2019 Expert Consensus From the Transplantion Society Working Group. *Transplantation* 104, 911–922. (2020). https://doi.org/10.1097/TP.0000000000003095
2. Papadimitriou, J. C. et al. Antibody-mediated allograft rejection: morphologic spectrum and serologic correlations in surveillance and for cause biopsies. *Transplantation* **95**, 128–136. https://doi.org/10.1097/TP.0b013e3182777f28 (2013).

3. Loupy, A. et al. The Banff 2019 Kidney Meeting Report (I): Updates on and clarification of criteria for T cell- and antibody-mediated rejection. *Am. J. Transpl.* **20**, 2318–2331. https://doi.org/10.1111/ajt.15898 (2020).
4. Rotman, S., Collins, A. B. & Colvin, R. B. C4d deposition in allografts: Current concepts and interpretation. *Transplantation reviews*. **19**, 65–77 (2005).
5. Zhang, X. & Reed, E. F. Effect of antibodies on endothelium. *Am. J. Transpl.* **9**, 2459–2465. https://doi.org/10.1111/j.1600-6143.2009.02819.x (2009).
6. Farkash, E. A. & Colvin, R. B. Diagnostic challenges in chronic antibody-mediated rejection. *Nat. Rev. Nephrol.* **8**, 255–257. https://doi.org/10.1038/nrneph.2012.61 (2012).
7. Sis, B. et al. Endothelial gene expression in kidney transplants with alloantibody indicates antibody-mediated damage despite lack of C4d staining. *Am. J. Transpl.* **9**, 2312–2323. https://doi.org/10.1111/j.1600-6143.2009.02761.x (2009).
8. Loupy, A., Mengel, M. & Haas, M. Thirty years of the International Banff Classification for Allograft Pathology: the past, present, and future of kidney transplant diagnostics. *Kidney Int.* **101**, 678–691. https://doi.org/10.1016/j.kint.2021.11.028 (2022).
9. Haas, M. et al. The Banff 2017 Kidney Meeting Report: Revised diagnostic criteria for chronic active T cell-mediated rejection, antibody-mediated rejection, and prospects for integrative endpoints for next-generation clinical trials. *Am. J. Transpl.* **18**, 293–307. https://doi.org/10.1111/ajt.14625 (2018).
10. Rosales, I. A. et al. Banff Human Organ Transplant Transcripts Correlate with Renal Allograft Pathology and Outcome: Importance of Capillaritis and Subpathologic Rejection. *J. Am. Soc. Nephrol.* **33**, 2306–2319. https://doi.org/10.1681/ASN.2022040444 (2022).
11. Margeta, D. et al. Spatial transcriptomics of Glomerulo-centric antibody mediated rejection in renal transplants. *Clin. Immunol.* **274**, 110460. https://doi.org/10.1016/j.clim.2025.110460 (2025).
12. Kang, M. et al. Spatial Transcriptomic Signatures of Early Acute T Cell-mediated Rejection in Kidney Transplants. *Transpl. Direct*. **10**, e1705. https://doi.org/10.1097/TXD.0000000000001705 (2024).
13. Mengel, M. et al. Banff 2019 Meeting Report: Molecular diagnostics in solid organ transplantation-Consensus for the Banff Human Organ Transplant (B-HOT) gene panel and open source multicenter validation. *Am. J. Transpl.* **20**, 2305–2317. https://doi.org/10.1111/ajt.16059 (2020).
14. Halloran, P. F. et al. Review: The transcripts associated with organ allograft rejection. *Am. J. Transpl.* **18**, 785–795. https://doi.org/10.1111/ajt.14600 (2018).
15. Halloran, P. F. et al. Real Time Central Assessment of Kidney Transplant Indication Biopsies by Microarrays: The INTERCOMEX Study. *Am. J. Transpl.* **17**, 2851–2862. https://doi.org/10.1111/ajt.14329 (2017).
16. Loupy, A. et al. The Banff 2015 Kidney Meeting Report: Current Challenges in Rejection Classification and Prospects for Adopting Molecular Pathology. *Am. J. Transpl.* **17**, 28–41. https://doi.org/10.1111/ajt.14107 (2017).

17. Muczynski, K. A., Ekle, D. M., Coder, D. M. & Anderson, S. K. Normal human kidney HLA-DR-expressing renal microvascular endothelial cells: characterization, isolation, and regulation of MHC class II expression. *J. Am. Soc. Nephrol.* **14**, 1336–1348. https://doi.org/10.1097/01.asn.0000061778.08085.9f (2003).
18. Clair, G. et al. The spatially resolved transcriptome signatures of glomeruli in chronic kidney disease. *JCI Insight*. **9** https://doi.org/10.1172/jci.insight.165515 (2024).
19. Siu, J. H. Y., Surendrakumar, V., Richards, J. A. & Pettigrew, G. J. T cell Allorecognition Pathways in Solid Organ Transplantation. *Front. Immunol.* **9**, 2548. https://doi.org/10.3389/fimmu.2018.02548 (2018).
20. Varin, A. et al. A Subset of Pro-inflammatory CXCL10 + LILRB2+ Macrophages Derives From Recipient Monocytes and Drives Renal Allograft Rejection. *Adv. Sci. (Weinh)*. **13**, e21294. https://doi.org/10.1002/advs.202521294 (2026).
21. Shah, Y. et al. Transcriptomic signatures of chronic active antibody-mediated rejection deciphered by RNA sequencing of human kidney allografts. *Kidney Int.* **105**, 347–363. https://doi.org/10.1016/j.kint.2023.11.012 (2024).
22. Teng, M. S. et al. A human TAPBP (TAPASIN)-related gene, TAPBP-R. *Eur. J. Immunol.* **32**, 1059–1068. https://doi.org/10.1002/1521-4141(200204)32:4%3C1059::AID-IMMU1059%3E3.0.CO;2-G (2002).
23. Wang, S. et al. Endothelial Cells in Antibody-Mediated Rejection of Kidney Transplantation: Pathogenesis Mechanisms and Therapeutic Implications. *J Immunol Res* 8746303. (2017). https://doi.org/10.1155/2017/8746303 (2017).
24. Louis, K. et al. Markers of graft microvascular endothelial injury may identify harmful donor-specific anti-HLA antibodies and predict kidney allograft loss. *Am. J. Transpl.* **19**, 2434–2445. https://doi.org/10.1111/ajt.15340 (2019).
25. Vonbrunn, E. et al. Multiplex gene analysis reveals T-cell and antibody-mediated rejection-specific upregulation of complement in renal transplants. *Sci. Rep.* **11**, 15464. https://doi.org/10.1038/s41598-021-94954-3 (2021).
26. Mulder, K. et al. Cross-tissue single-cell landscape of human monocytes and macrophages in health and disease. *Immunity* **54**, 1883–1900. https://doi.org/10.1016/j.immuni.2021.07.007 (2021). e1885.
27. Lei, Y. et al. Receptor-2 Drive Alloimmunity and Immune Regulation in Kidney Allograft Rejection. *Front. Cell. Dev. Biol.* **8**, 398. https://doi.org/10.3389/fcell.2020.00398 (2020). Cathepsin S and Protease-Activated.
28. Cross, A. R., Glotz, D. & Mooney, N. The Role of the Endothelium during Antibody-Mediated Rejection: From Victim to Accomplice. *Front. Immunol.* **9**, 106. https://doi.org/10.3389/fimmu.2018.00106 (2018).
29. Van Loon, E. et al. Active immunologic participation and metabolic shutdown of kidney structural cells during kidney transplant rejection. *Am. J. Transpl.* **25**, 531–544.

https://doi.org/10.1016/j.ajt.2024.10.015 (2025).

30. Naesens, M. et al. The Banff 2024 Kidney Meeting Report: Rejection as a spectrum of phenotypes and focus on differential diagnostic reasoning. *Am. J. Transpl.* **26**, 922–936. https://doi.org/10.1016/j.ajt.2026.01.018 (2026).
31. Madill-Thomsen, K. et al. Discrepancy analysis comparing molecular and histology diagnoses in kidney transplant biopsies. *Am. J. Transpl.* **20**, 1341–1350. https://doi.org/10.1111/ajt.15752 (2020).
32. Callemeyn, J. et al. Transcriptional Changes in Kidney Allografts with Histology of Antibody-Mediated Rejection without Anti-HLA Donor-Specific Antibodies. *J. Am. Soc. Nephrol.* **31**, 2168–2183. https://doi.org/10.1681/ASN.2020030306 (2020).

Figures

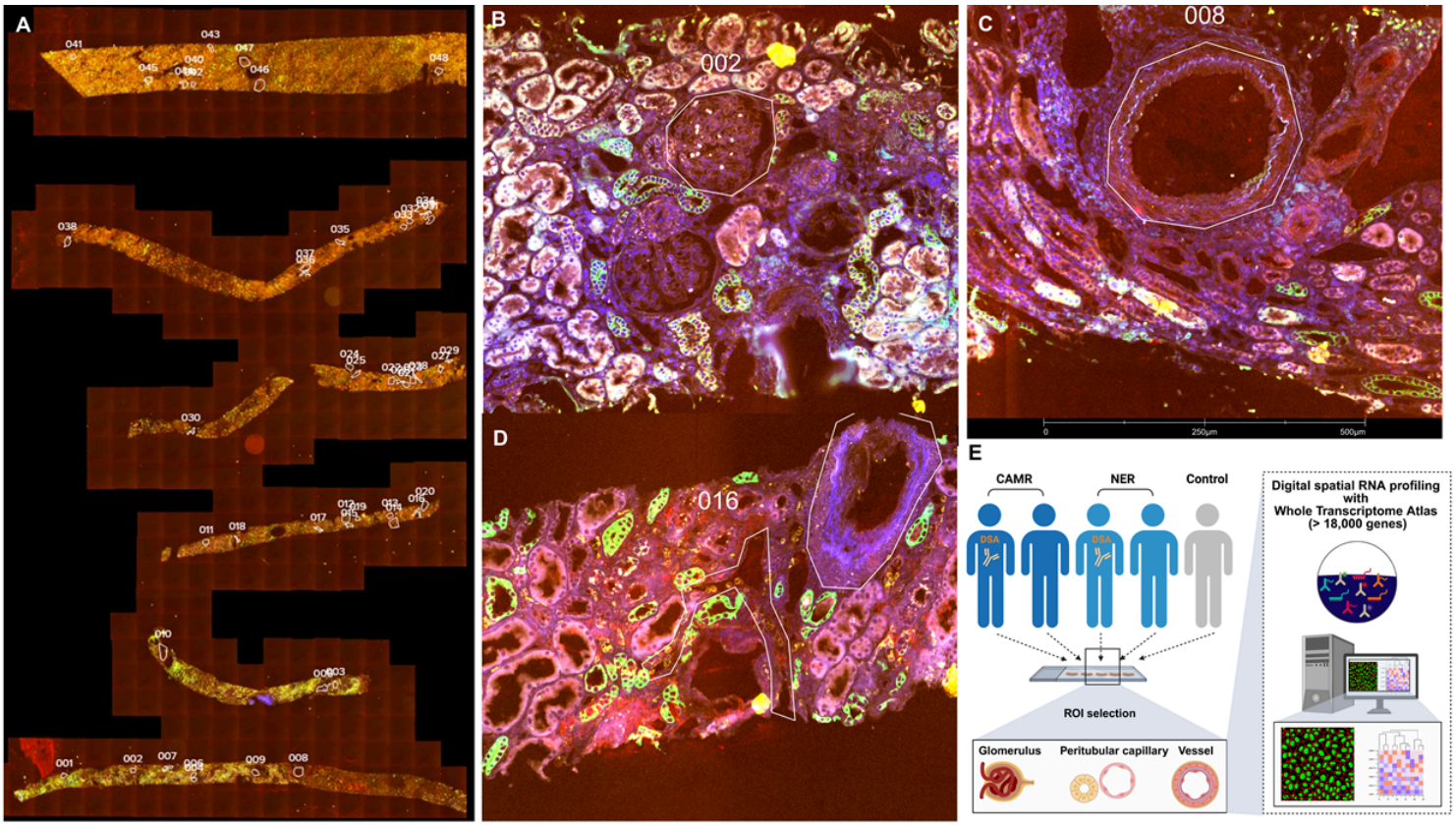


Figure 1

Immunofluorescence images of four renal allografts and a control kidney used in the GeoMx digital spatial profiling (DSP) analysis.

(A) From bottom to top: donor-specific antibody (DSA)-positive chronic antibody-mediated rejection (CAMR), DSA-negative CAMR, DSA-positive no evidence of rejection (NER), DSA-negative NER, and control tissue. Representative ROI images containing a glomerulus **(B)**and an artery **(C)** in DSA-positive

CAMR, and peritubular capillaries **(D)**in DSA-negative CAMR (×200). Green, PanCK; yellow, CD45; red, CD31; blue, SYTO13 (nuclei). **(E)** Schematic overview of the study. Created with BioRender (Jung, J., 2026; https://BioRender.com/ole77bw).

CAMR, chronic antibody-mediated rejection; DSA, donor-specific antibody; NER, no evidence of rejection; ROI, regions of interest.

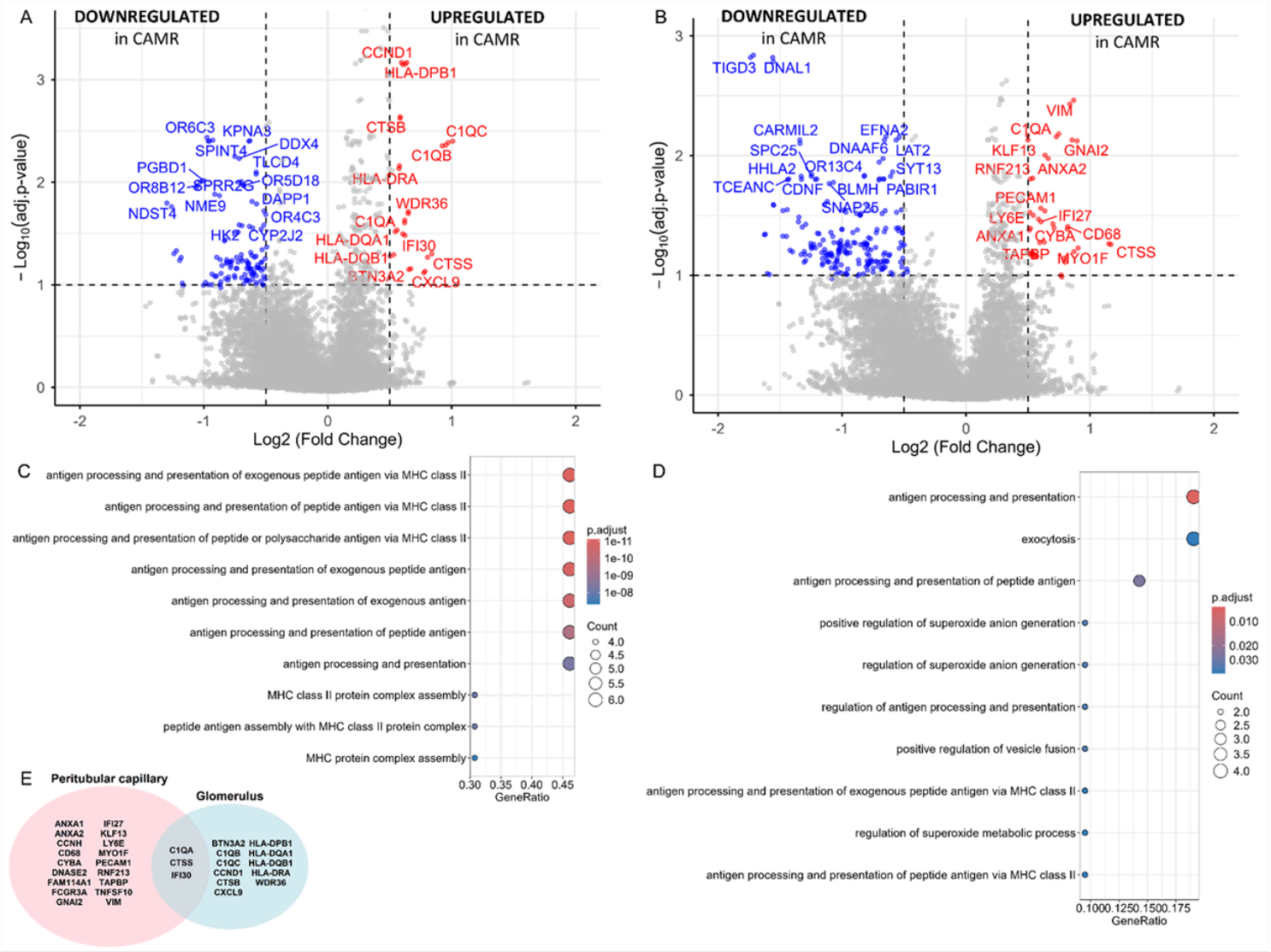


Figure 2

Higher expression of antigen processing and presentation-related genes was observed in the glomerular and peritubular capillary ROIs in CAMR compared to non-CAMR.

A&B. Volcano plots showing significantly upregulated (red) and downregulated (green) genes in CAMR compared to the non-CAMR biopsies. Glomerular (A) CAMR ROIs (n=8; 4 DSA-positive, 4 DSA-negative) compared with non-CAMR glomerular ROIs (n=10; 4 DSA-positive NER, 3 DSA-negative NER, and 3 controls). Peritubular capillary (B) ROIs (n=6; 3 DSA-positive, 3 DSA-negative) compared with non-CAMR ROIs (n=9; 3 DSA-positive NER, 3 DSA-negative NER, and 3 controls). For visualization purposes, the x-

axis was symmetrically centered at zero, and extreme log2 fold-change values were capped; no genes were excluded from the analysis. Only the top 15 genes were labeled by symbol.

C&D. Gene ontology biological process terms enriched among genes upregulated in CAMR glomerular (C) ROIs and peritubular capillary (D) ROIs.

E. Overlap of significantly upregulated genes in glomerular peritubular capillary ROIs in CAMR compared to non-CAMR biopsies.

CAMR, chronic antibody-mediated rejection; ROI, regions of interest; DSA, donor-specific antibody; NER, no evidence of rejection.

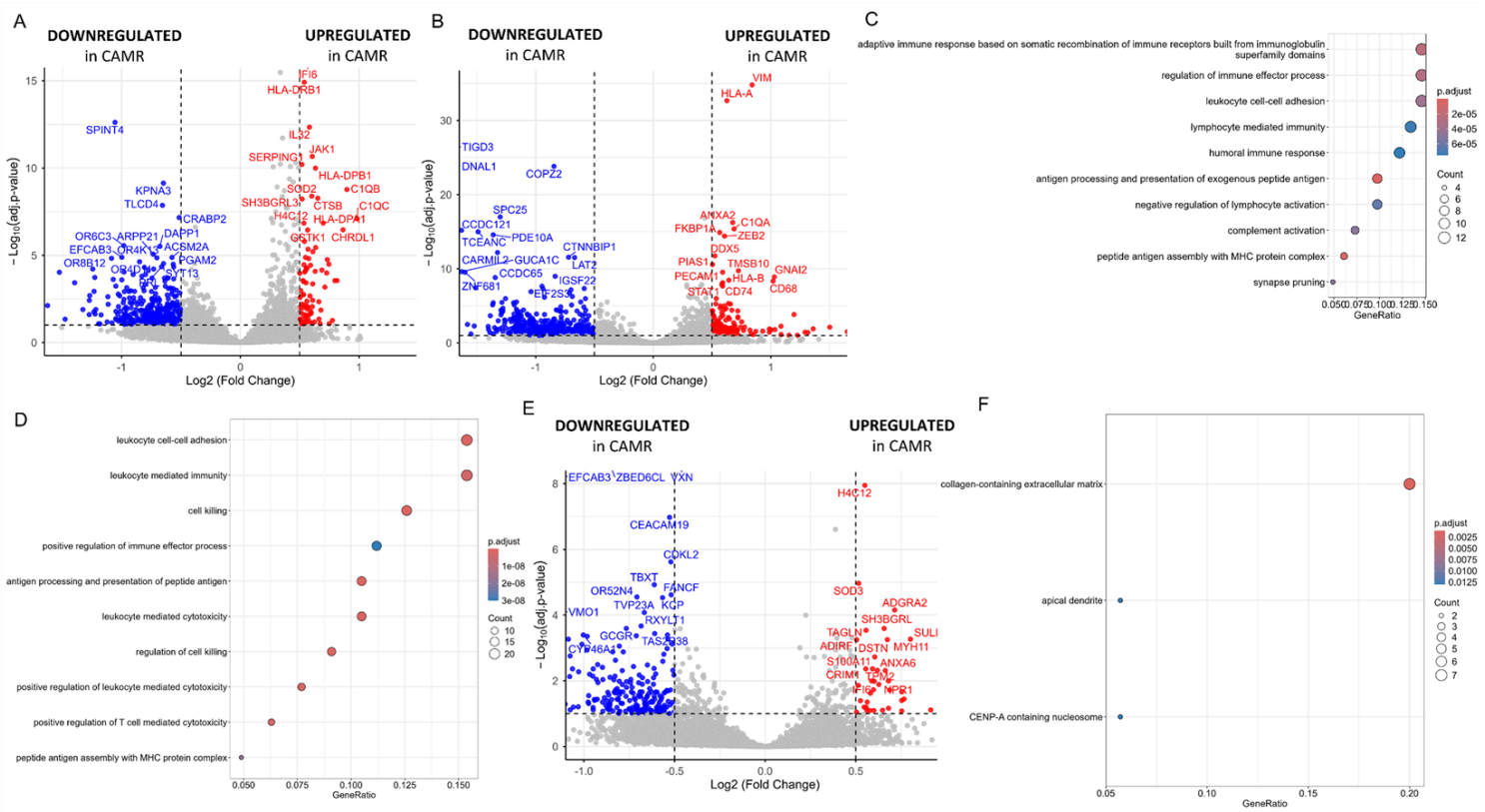


Figure 3

LMM analysis restricted to allograft ROIs expands DEG detection and reveals vascular remodeling signature in CAMR.

A&B. Volcano plots showing significantly upregulated (red) and downregulated (blue) genes in CAMR compared to the NER biopsies. Glomerular **(A)** CAMR ROIs (n=8; 4 DSA-positive, 4 DSA-negative) compared with NER glomerular ROIs (n=7; 4 DSA-positive NER, 3 DSA-negative NER). Peritubular capillary **(B)** ROIs (n=6; 3 DSA-positive, 3 DSA-negative) compared with non-CAMR ROIs (n=6; 3 DSA-positive NER, 3 DSA-negative NER). For visualization purposes, the x-axis was symmetrically centered at zero, and extreme log2 fold-change values were capped; no genes were excluded from the analysis. Only the top 15 genes were labeled by symbol.

C&D. Gene ontology biological process terms enriched among genes upregulated in CAMR glomerular **(C)** ROIs and peritubular capillary **(D)** ROIs.

E. Volcano plot showing significantly upregulated (red) and downregulated (blue) genes in CAMR (n=6; 3 DSA-positive, 3 DSA-negative) compared to the NER (n=6; 3 DSA-positive NER, 3 DSA-negative NER) biopsies in vascular ROIs.
F. Gene ontology cellular component terms enriched among genes upregulated in CAMR vascular ROIs (n=6; 3 DSA-positive, 3 DSA-negative) compared to NER ROIs (n=6; 3 DSA-positive NER, 3 DSA-negative NER).

LMM, linear mixed model; DEG, differentially expressed genes; ROI, regions of interest; CAMR, chronic antibody-mediated rejection; DSA, donor-specific antibody; NER, no evidence of rejection.

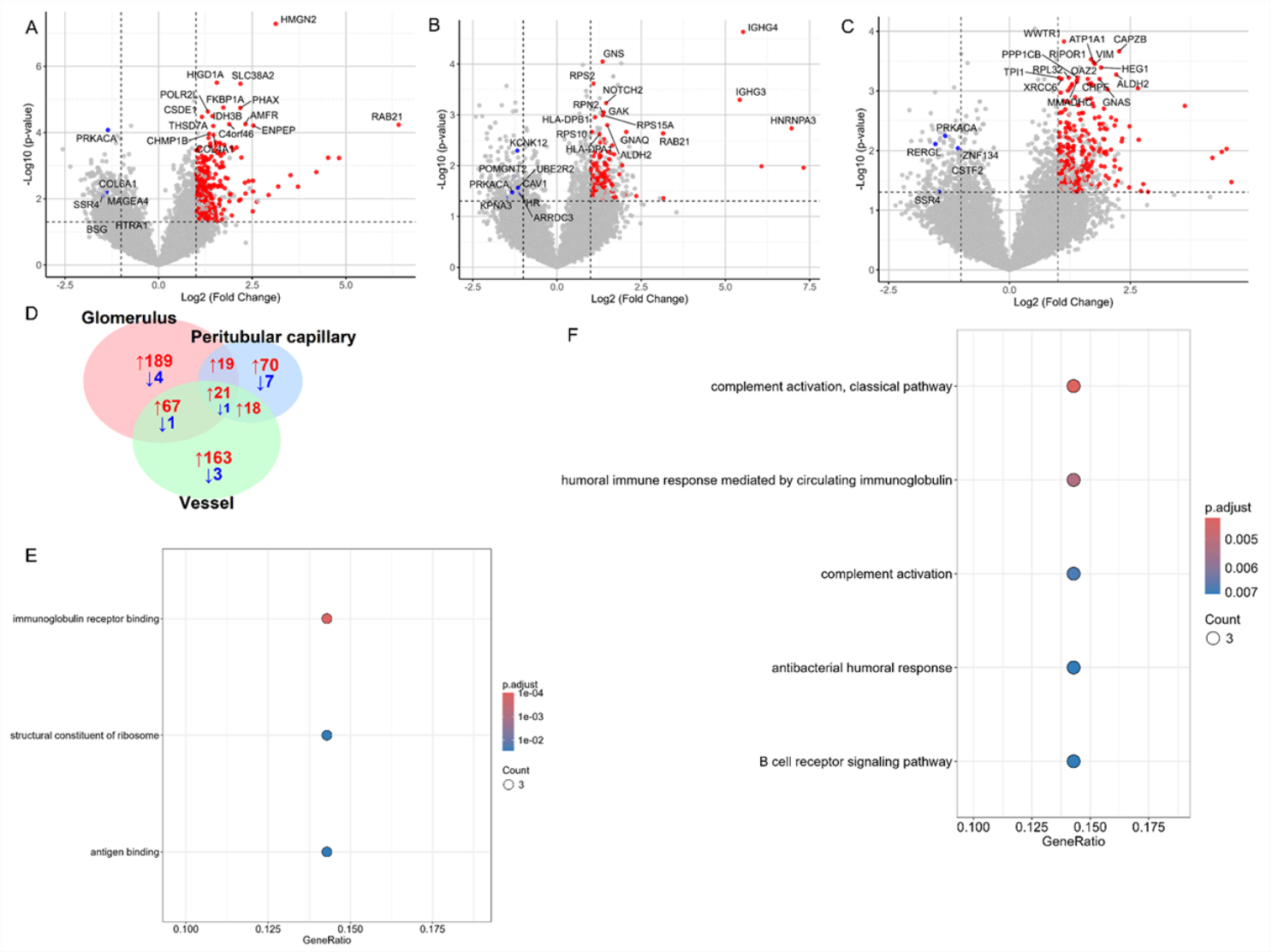


Figure 4

Increased expression of genes associated with classical complement activation was observed in the glomerular, peritubular capillary, and vascular ROIs in DSA-positive CAMR compared to DSA-negative

CAMR.

A–C. Volcano plots showing significantly upregulated (red) and downregulated (blue) genes in DSA-positive CAMR compared to DSA-negative CAMR in the glomerular **(A),** peritubular capillary **(B),** and vascular **(C)** compartments. **(D)** Venn diagram showing compartment-specific differentially expressed genes between DSA-positive and DSA-negative CAMR. Red and blue numbers represent upregulated and downregulated genes, respectively. **E&F.** Gene ontology analysis of genes commonly upregulated in DSA-positive CAMR across glomerular, peritubular capillary, and vascular ROIs: molecular functions **(E)** and biological processes **(F).**

CAMR, chronic antibody-mediated rejection; DSA, donor-specific antibody; ROI, regions of interest.

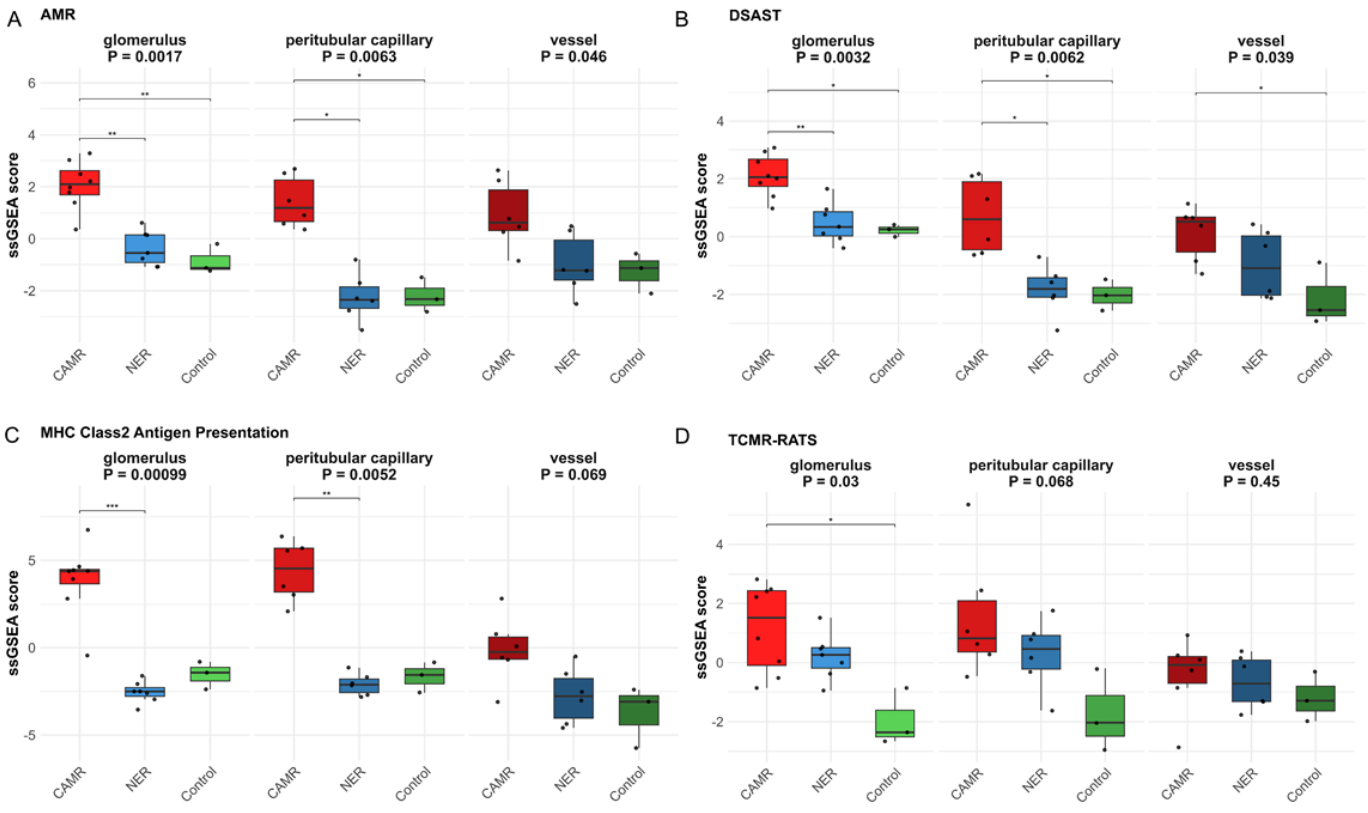


Figure 5

Dot plot of single sample gene set enrichment analysis (ssGSEA) scores for each B-HOT pathway by renal compartment.

Each dot represents the ssGSEA score of an individual ROI. The pathways associated with antibody-mediated rejection (AMR) **(A)**, donor-specific antibody-associated tissue signatures (DSAST) **(B)**, and MHC class II antigen presentation **(C)** consistently showed higher scores in CAMR compared to NER and control across all compartments, except that the MHC class II antigen presentation score in the vascular compartment showed an increasing trend that did not reach statistical significance (p=0.069). In contrast, T cell–mediated rejection-related acute tissue signatures (TCMR-RATS) scores (**D**) do not

display significant differences between the CAMR and NER groups in any renal compartment. * p<0.05, ** p<0.01, *** p<0.001.

AMR, antibody-mediated rejection; DSAST, donor-specific antibody-associated tissue signatures; TCMR-RATS, T cell-mediated rejection-related acute tissue signatures; ROI, region of interest; CAMR, chronic active antibody-mediated rejection; NER, no evidence of rejection.

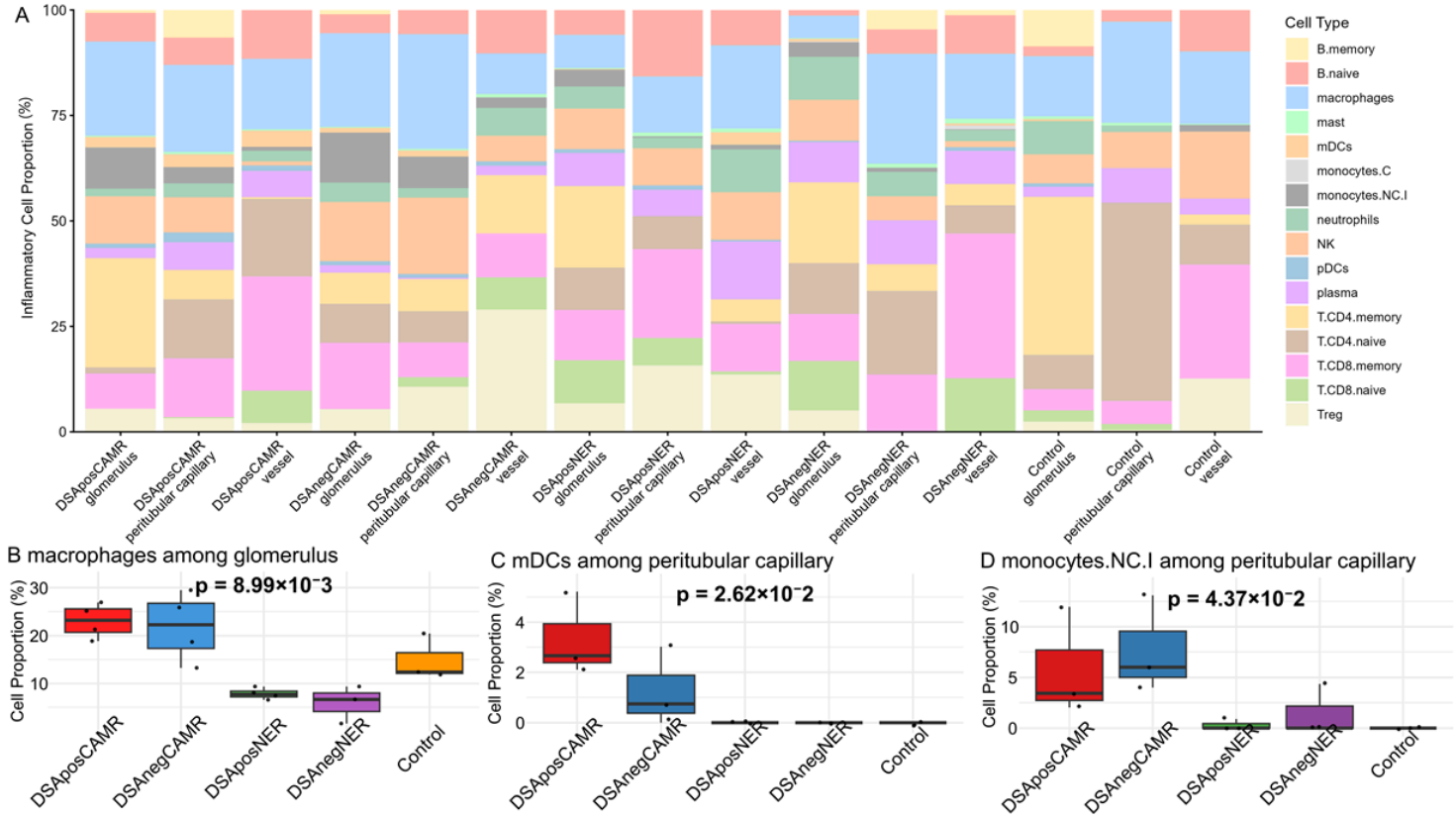


Figure 6

Spatial deconvolution of inflammatory cells across ROIs.

(A) Distribution of inflammatory cell types according to diagnosis and renal compartments. **(B)** In the comparison of the glomerular ROI, the CAMR groups exhibited a greater proportion of macrophages than the non-CAMR groups. In the comparison of peritubular capillary ROIs, the CAMR groups showed increased proportions of myeloid dendritic cells and non-classical intermediate monocytes relative to the non-CAMR groups. **(C)** The proportion of myeloid dendritic cells was higher in the DSA-positive CAMR group, whereas **(D)** the proportion of non-classical/intermediate monocytes was higher in the DSA-negative CAMR group.

CAMR, chronic antibody-mediated rejection; DSA, donor-specific antibody; mDCs, myeloid dendritic cells;monocytes.C, classical monocytes; monocytes.NC.I., non-classical/intermediate monocytes; NER, no evidence of rejection; NK, natural killer, pDCs, plasmacytoid dendritic cells; ROI, region of interest; Treg, regulatory T cells.

Supplementary Files

This is a list of supplementary files associated with this preprint. Click to download.

- SupplementaryFigures.pdf
- Supplementarymethod.pdf
- SupplementaryTableS1.docx